Available online at www.sciencedirect.com
ScienceDirect
Journal of Sound and Vibration 313 (2008) 784–805
JOURNAL OF SOUND AND VIBRATION
www.elsevier.com/locate/jsvi

Nonlinear frequency responses of quarter vehicle models with amplitude-sensitive engine mounts

Jun Hwa Lee, Rajendra Singh*

Acoustics and Dynamics Laboratory, Department of Mechanical Engineering, The Ohio State University, Columbus, OH 43210, USA

Received 16 August 2007; received in revised form 15 November 2007; accepted 3 December 2007
Available online 9 January 2008

Abstract

Although the amplitude dependence of engine mounts has been widely studied via experimental and analytical studies, its effect on the vehicle system response is still unclear. Therefore, the chief goal of this paper is to develop a method that will incorporate measured dynamic stiffness properties of the isolator and predict the resulting amplitude-dependent nonlinear behavior of the governing system in the frequency domain. Experimental data on two hydraulic engine mount concepts, namely the inertia track and free decoupler mounts, are incorporated to illustrate realistic amplitude dependence. Then, nonlinear frequency responses of two quarter vehicle models, up to 50 Hz, are analytically calculated using the one-term harmonic balance method. Our analysis shows that the proposed semi-analytical scheme should be employed, instead of *ad hoc* methods, when the mount parameters are amplitude-sensitive. In particular, the inclusion of inertia track mount leads to the softening effect. A comparison with Duffing's oscillator is made to qualitatively assess its nature. A system with the free decoupler mount looks more like a linear time-invariant system, at least from the frequency response perspective, due to high decoupler damping that negates the amplitude sensitivity. Finally, some numerical convergence issues are briefly discussed.

1. Introduction

Many practical isolators such as engine mounts, suspension bushings and the like exhibit significant nonlinearities and their visco-elastic properties depend on the amplitude and frequency of dynamic excitation, static load, and temperature [1–13]. It is often difficult to analytically model such devices and thus experimental approaches must be adopted for dynamic characterization. For instance, consider the non-resonant elastomer test, where the isolator or mount is evaluated at a given frequency ω (rad/s) and peak-to-peak (p–p) amplitude X of sinusoidal displacement excitation, under a specific static load f_s (or displacement). Isolation component suppliers routinely measure the cross-point dynamic stiffness $K(\omega, X) = F_T/X$ where F_T is the amplitude (p–p) of the force transmitted to a rigid base only at the ω though super- and sub-harmonics might be present [3,4]. These experiments on hydraulic engine mounts (example of this article) clearly exhibit highly nonlinear characteristics as K significantly varies with X and ω of sinusoidal excitation [2–5]. Mount characteristics have, usually in the form of $K(\omega, X)$, been extensively investigated, based on experimental and

*Corresponding author. Tel.: +1 614 292 9044; fax: +1 614 292 3163.
E-mail address: singh.3@osu.edu (R. Singh).

0022-460X/$ - see front matter © 2007 Elsevier Ltd. All rights reserved.
doi:10.1016/j.jsv.2007.12.006

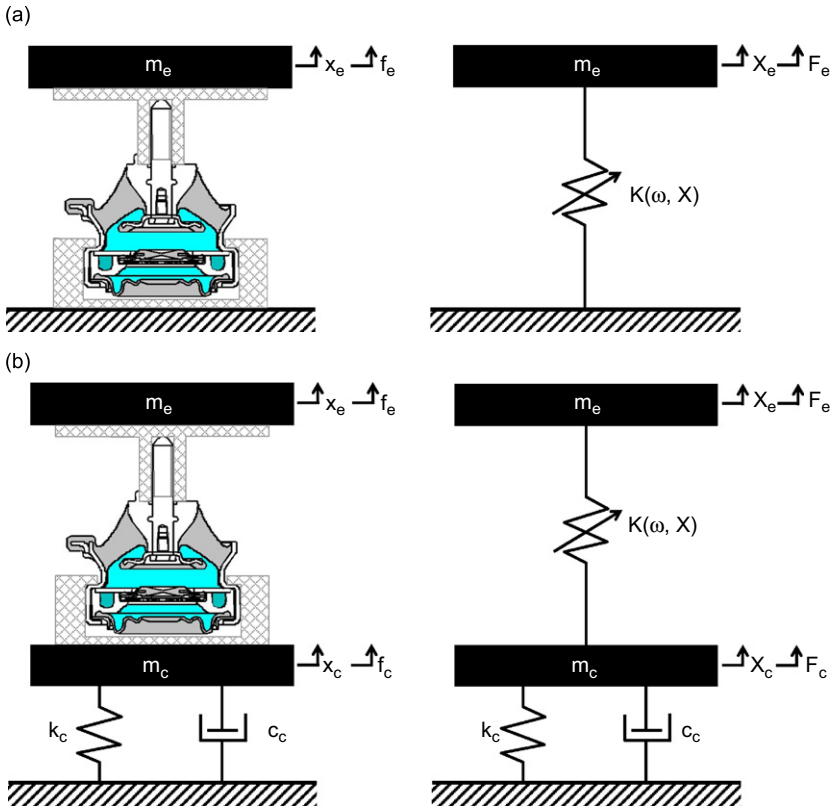

Fig. 1. Quarter vehicle models: (a) System A: engine–mount system and (b) system B: engine–mount–chassis system.

analytical studies [2–12]. But their incorporation into vehicle system models is not well understood [7]. Researchers and practitioners have adopted a few *ad hoc* treatments including a lookup table scheme that allows them to pick constant visco-elastic parameters. Further, curve fits have been used to define spectral variations but amplitude dependence is often ignored. This paper will specifically discuss the inclusion of $K(\omega, X)$ in two quarter vehicle models that are depicted in Fig. 1 and then construct nonlinear frequency responses by using the method of harmonic balance (HBM).

2. Problem formulation

2.1. Unresolved research issues

First, one must carefully examine the definition of peak-to-peak amplitude X, in the non-resonant mount test [13], as the isolator is always placed between two sub-systems. For instance, consider system A of Fig. 1(a) that consists of engine mass m_e, hydraulic engine mount and rigid base. In this case, X can be determined only when the displacement of engine x_e is known. Essentially, X is the p–p amplitude of x_e when the external excitation f_e is sinusoidal like the mount test. Conversely, when the isolator is installed between two dynamic sub-systems as in system B of Fig. 1(b), X is not known until both engine and chassis displacements, x_e and x_c, are calculated. Here, m_c is the mass of chassis; k_c and c_c are the stiffness and damping coefficients of chassis; x_c is the displacement of chassis; and f_c is the external force applied to chassis. Thus, X should be regarded as the amplitude of relative displacement for system B, while it is the amplitude of absolute displacement for system A.

Second, examine the nature of governing equations. For the sake of illustration, the equation of motion for system A is sometimes inadvertently written as follows:

$$m_e\ddot{x}_e(t) + K(\omega, X)x_e(t) = f_e(t). \tag{1}$$

Note that Eq. (1) is not a true ordinary differential equation since the meanings (or consequences) of ω and X are unclear. Consequently, the transformation of $K(\omega, X)$ from frequency to time domain is indeterminate and could be unrealistic. However, Eq. (1) could be applied (just like the structural damping formulations [14]) when the external force $f_e(t)$ is harmonic, such as $f_e(t) = F_e \cos \omega t$. In this case, the meaning of ω becomes clear and X is related to the amplitude (zero to peak) of $x_e(t)$, as $X = X_e$ when both are peak-to-peak, assuming that $x_e(t) = X_e \cos(\omega t - \varphi_e)$. Further, X_e should be determined by means of an iterative technique such as the Newton–Raphson method (our method as discussed later). Therefore, the one-term harmonic balance (or describing function) method could be effectively employed to obtain the frequency response of a system with amplitude-sensitive and spectrally varying parameters; this is the basis of our analysis. This approach is consistent with steady-state elastomer tests where $K(\omega, X)$ data are measured only at given ω [4–9]; essentially the method of one-term harmonic balance is experimentally implemented.

Third, researchers have attempted to faithfully characterize the following nonlinearities of hydraulic engine mounts: nonlinear chamber compliances [13,15], vacuum formation in the upper chamber during the expansion process [4,15], nonlinear resistances of the inertia track and decoupler [13,15], and switching mechanism of the decoupler [13,15]. Such characterizations require a series of dedicated laboratory experiments [4,6,13]. Such experiments are often time-consuming and suitable for academic research but often impractical for vehicle manufacturers as they may possess hundreds of nonlinear devices. Thus, one must find a way to utilize off the shelf data for real-life devices, in the form of $K(\omega, X)$, from the component suppliers. This would lead to an efficient vehicle dynamic analysis, and yet yield information on the amplitude sensitivity from the noise and vibration control, vehicle ride or durability perspective.

2.2. Ad hoc methods

One particular *ad hoc* method employs a lookup table scheme which is used to estimate a constant stiffness (k) and a constant viscous damping (c) coefficients from the measured $K(\omega, X)$ data. The analyst typically assumes that certain frequency and typical amplitude values are of interest based on particular vehicle problems or conditions. The resulting linear time-invariant model can then be easily dealt with in both time and frequency domains. Also, the eigenvalue problem can be posed. Despite its mathematical ease, this approach yields amplitude-independent system responses and thus raises questions on its utility. This analysis is indeed valid only at the frequency and the amplitude where k and c values were selected.

Yet in another *ad hoc* approach, $K(\omega, X)$ is approximated by $K(\omega)$ by assuming a typical amplitude. The mathematical treatment with the spectrally varying stiffness is straightforward in frequency domain, although the corresponding time-domain formulation cannot be exactly formulated. In addition, the spectrally varying nature of stiffness could lead to ambiguous eigensolutions of a system. However, if a causal transfer function is to be constructed to faithfully describe $K(\omega)$ in the Laplace domain, the time-domain formulation can be derived by the inverse Laplace transform method. In the case of hydraulic engine mounts, this method leads to a linear ordinary differential equation (with real time-invariant coefficients) of third or higher order. This implies that one or more "artificial" degrees of freedom are introduced and complex-valued eigensolutions can be found without any difficulty. Unlike the lookup table scheme that works at only one frequency, the curve-fit method predicts responses over a frequency range. But, the amplitude sensitivity of the system response cannot be found. Accordingly, a careful interpretation is required when the isolator is highly amplitude-sensitive.

2.3. Scope and objectives

Although the amplitude dependence of mounts or isolators has been widely studied via experimental and analytical studies [2–12], its effect on the system response is still unclear to the best of our knowledge. Therefore, the chief goal is to develop a method that will incorporate $K(\omega, X)$ data of the isolator and predict the nonlinear behavior of a system. Dynamic analysis is restricted to the frequency domain only, up to 50 Hz. Experimental data on the two hydraulic mount concepts, namely the inertia track and free decoupler mounts, will be incorporated to illustrate realistic amplitude dependence. The range of displacement excitation amplitude (X) is from 0.3 mm (p–p) to 3.0 mm (p–p) for the inertia track mount and from 1.0 mm (p–p) to

3.0 mm (p–p) for the free decoupler mount. Nonlinear frequency responses of two quarter vehicle models, systems A and B of Fig. 1, are calculated, based on the premise that only limited measurements of $K(\omega, X)$ are available. The one-term harmonic balance method is employed for the semi-analytical characterization of system A or B with a nonlinear component. Some results for system A will be given later to illustrate how the *ad hoc* techniques (as discussed earlier) might fail. Although the time-domain integration schemes (such as the Runge–Kutta method) are commonly used to validate the harmonic balance method, they are not applicable in our case since specific nonlinear amplitude-dependent differential equations cannot be defined. Instead, we will also compare the backbone curves of the nonlinear frequency responses with that given by Duffing's oscillator to qualitatively assess their nature. Furthermore, some numerical convergence issues are briefly discussed.

3. Semi-analytical solutions for systems with inertia track mount

3.1. Quasi-linear model of inertia track mount

The fluid model of a hydraulic engine mount with inertia track and free decoupler as shown in Fig. 2 is briefly reviewed here in order to derive a curve-fit function for the quasi-linear model. Detailed description of the model and its experimental validation are given in Refs. [13,15]. For the fluid model of Fig. 2, k_r and c_r are the stiffness and damping coefficients of the rubber part, respectively; C_u and C_ℓ are the (linearized) fluid compliances of the upper (#u) and lower (#ℓ) chambers; $q_i(t)$ and $q_d(t)$ are the volumetric flow rates through the inertia track (#i) and decoupler (#d); I_i and I_d are the inertias of fluid columns; and R_i and R_d are the (linearized) fluid resistances. The dynamic component of driving point force $f(t)$ is expressed as follows:

$$f(t) = c_r\dot{x}(t) + k_r x(t) + A_p p_u(t), \tag{2}$$

where $x(t)$ is the dynamic displacement, A_p is the effective rubber (piston) area and $p_u(t)$ is the dynamic pressure of the upper chamber.

Continuity equations for the upper and lower chambers are written as follows:

$$A_p\dot{x}(t) - q_i(t) - q_d(t) = C_u\dot{p}_u(t), \tag{3}$$

$$q_i(t) + q_d(t) = C_\ell\dot{p}_\ell(t). \tag{4}$$

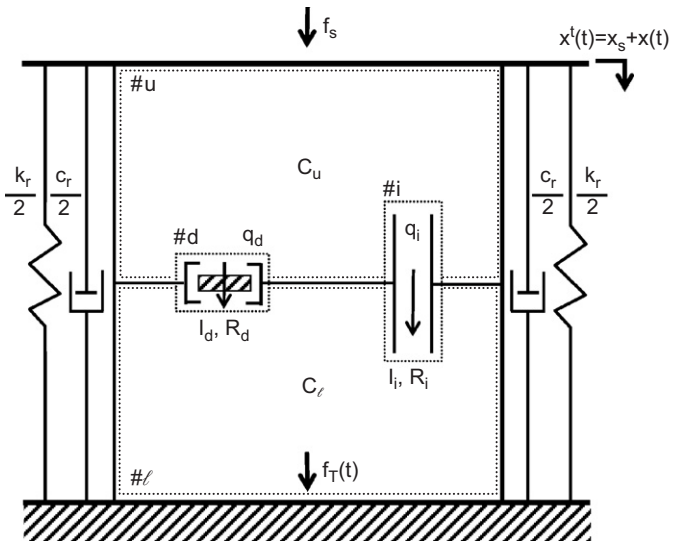

Fig. 2. Fluid model of the hydraulic engine mount with inertia track and free decoupler.

Momentum equations for the inertia track and decoupler are

$$p_u(t) - p_\ell(t) = I_i\dot{q}_i(t) + R_i q_i(t), \tag{5}$$

$$p_u(t) - p_\ell(t) = I_d\dot{q}_d(t) + R_d q_d(t). \tag{6}$$

The dynamic component of the force $f_T(t)$ transmitted to the rigid base is related to $f(t)$ as follows [16,17] since the effect of rubber mass is negligible up to 50 Hz:

$$f_T(t) = c_r\dot{x}(t) + k_r x(t) + A_p p_u(t) = f(t). \tag{7}$$

In the inertia track mount, the only path of the fluid flow between the upper and lower chambers is through the track. Accordingly, the transfer function can be derived from Eqs. (2), (3), (5), (7) with $q_d(t) = 0$ in the Laplace (s) domain as follows:

$$K(s) = \frac{F(s)}{X(s)} \quad \text{or} \quad \frac{F_T(s)}{X(s)} = k_r + c_r s + k_u \frac{m_{ie}s^2 + c_{ie}s}{m_{ie}s^2 + c_{ie}s + k_u}, \tag{8}$$

where k_u, m_{ie}, and c_{ie} are respectively defined as $k_u = A_p^2/C_u$, $m_{ie} = A_p^2 I_i$, and $c_{ie} = A_p^2 R_i$.

In comparison with $p_u(t)$, it is further assumed that the pressure in the lower chamber is nearly the same as the atmospheric pressure, that is, $p_\ell(t) \approx 0$, since the lower chamber compliance C_ℓ is very large in practice (rubber bellows).

Using Eq. (8), a quasi-linear model [18] could be estimated from $K(\omega, X)$ measurements as shown in Fig. 3(a). This leads to a quasi-linear formulation, but amplitude-dependent stiffness as defined below:

$$K(s, X) = k_r + c_r s + k_u(X) \frac{m_{ie}s^2 + c_{ie}s}{m_{ie}s^2 + c_{ie}s + k_u(X)}. \tag{9}$$

Fig. 3(b) shows the dynamic transfer stiffness by the quasi-linear model of Eq. (9) with the estimated parameters of Table 1 where k_u is the upper chamber stiffness; m_{ie} and c_{ie} are the equivalent mass and damping coefficient representing the inertia and damping effects by fluid flow through the inertia track. Although averaged values are taken except for k_u, the quasi-linear model is in an acceptable agreement with its corresponding measurement. For more information on the estimation procedure, refer to He and Singh's work [18].

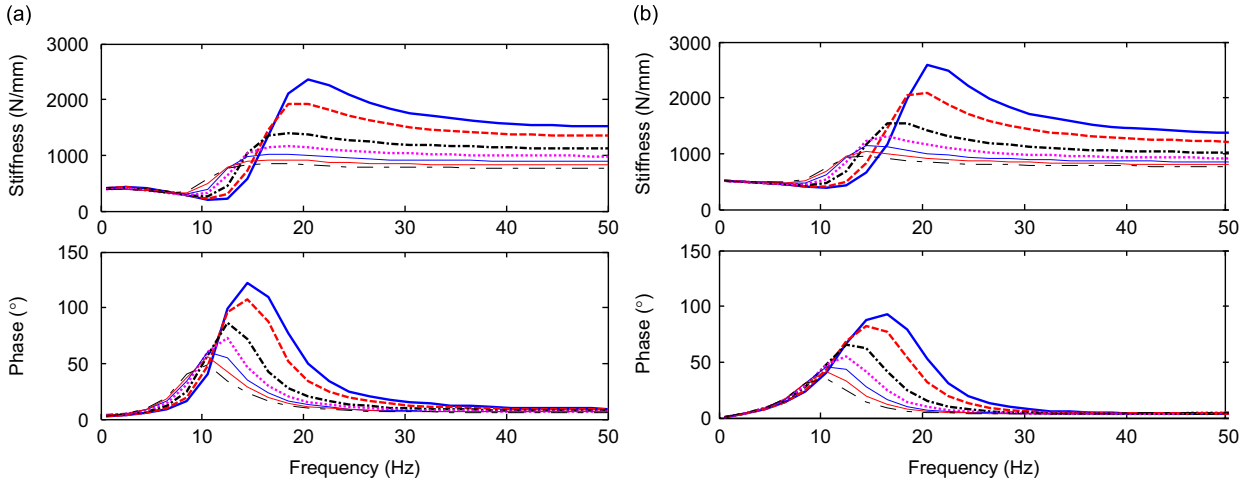

Fig. 3. Dynamic stiffness spectra of the inertia track mount: (a) measurements and (b) predicted by the quasi-linear model given in Eq. (9). Key: ——, $X = 0.3$ mm p–p; – – –, $X = 0.5$ mm p–p; — · —, $X = 1.0$ mm p–p; ·····, $X = 1.5$ mm p–p; ——, $X = 2.0$ mm p–p; - - - - - -, $X = 2.5$ mm p–p; —·—·—, $X = 3.0$ mm p–p.

The dependence of k_u (in N mm^{-1}) on X (in mm p–p) could be approximated by a polynomial curve fit of order n as

$$k_u(X) = \sum_{i=0}^{n} a_i X^i. \tag{10}$$

Fig. 4 shows the curve fits (from first- to fourth-order polynomials) to the given estimated parameters of Table 1. Table 2 compares the associated correlation coefficients (r). Although the second-order polynomial

Table 1
Amplitude-dependent parameters of the inertia track mount

	X (mm) p–p							
	0.3	0.5	1.0	1.5	2.0	2.5	3.0	Average
k_r (N mm^{-1})	528	535	534	513	494	475	468	507
c_r (N s m^{-1})	295	282	222	198	186	172	160	216
k_u (N mm^{-1})	726	610	459	376	319	281	246	–
c_{ie} (N s m^{-1})	2056	1964	2018	1971	1921	1923	1872	1961
m_{ie} (kg)	46.3	45.6	47.0	46.5	45.9	45.9	46.3	46.2

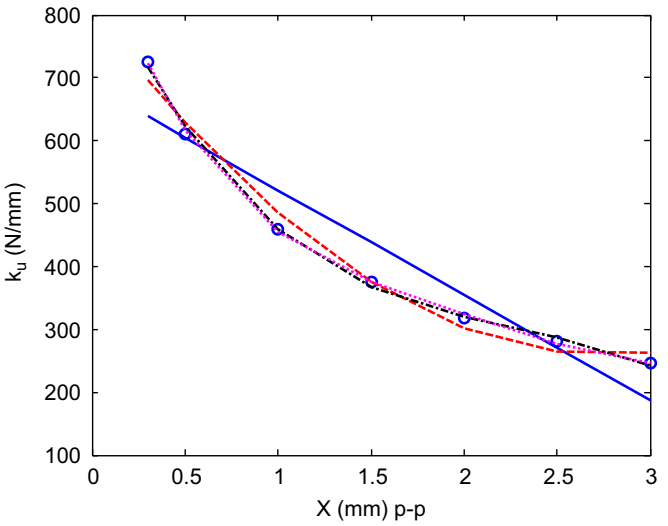

Fig. 4. Dependence of k_u on X. Key: ◯, estimated parameters of Table 1; ——, $k_u(X)$ of first-order polynomial; – – –, $k_u(X)$ of second-order polynomial; — · —, $k_u(X)$ of third-order polynomial; ·····, $k_u(X)$ of fourth-order polynomial.

Table 2
Polynomial coefficients of k_u for the inertia track mount, along with r values

	$n=1$	$n=2$	$n=3$	$n=4$
a_0	688.4	809.9	888.6	947.0
a_1	−166.8	−395.8	−648.4	−903.2
a_2		71.0	256.9	568.9
a_3			−37.5	−179.2
a_4				21.3
r	0.9459	0.9930	0.9989	0.9997

looks reasonable, we will proceed with the third-order polynomial. As discussed later, our investigation revealed that the convergence during the iteration process was polynomial-order dependent.

3.2. Equation of motion for system A

Consider the system A as shown in Fig. 1(a), which is apparently a single-degree-of-freedom system but the second degree of freedom is brought in by the mount dynamics. The governing equations are as follows:

$$m_e\ddot{x}_e + f_H = f_e, \tag{11}$$

where f_H is the internal hydraulic force generated by the engine mount.

Now define the transfer function in the Laplace domain as

$$\frac{F_H(s)}{X_e(s)} = K(s,X) = k_r + c_r s + k_u(X)\frac{m_{ie}s^2 + c_{ie}s}{m_{ie}s^2 + c_{ie}s + k_u(X)}. \tag{12}$$

Rewrite Eq. (12) as follows

$$m_{ie}\ddot{f}_H + c_{ie}\dot{f}_H + k_u(X)f_H = m_{ie}c_r\dddot{x}_e + \mu(X)\ddot{x}_e + \gamma(X)\dot{x}_e + k_u(X)k_r x_e, \tag{13}$$

where $\mu(X) = m_{ie}k_r + c_r c_{ie} + m_{ie}k_u(X)$ and $\gamma(X) = k_r c_{ie} + k_u(X)c_r + k_u(X)c_{ie}$.

Express Eqs. (11) and (13) in a matrix form as

$$\begin{bmatrix} 0 & 0 \\ -m_{ie}c_r & 0 \end{bmatrix}\begin{bmatrix} \dddot{x}_e \\ \dddot{f}_H \end{bmatrix} + \begin{bmatrix} m_e & 0 \\ -\mu(X) & m_{ie} \end{bmatrix}\begin{bmatrix} \ddot{x}_e \\ \ddot{f}_H \end{bmatrix} + \begin{bmatrix} 0 & 0 \\ -\gamma(X) & c_{ie} \end{bmatrix}\begin{bmatrix} \dot{x}_e \\ \dot{f}_H \end{bmatrix} + \begin{bmatrix} 0 & 1 \\ -k_u(X)k_r & k_u(X) \end{bmatrix}\begin{bmatrix} x_e \\ f_H \end{bmatrix} = \begin{bmatrix} f_e \\ 0 \end{bmatrix}. \tag{14}$$

Eqs. (11)–(14) could be valid only when the external force f_e is sinusoidal, that is, $f_e = F_{e0} + F_{es}\sin\omega t + F_{ec}\cos\omega t$. Assume that $x_e = X_{e0} + X_{es}\sin\omega t + X_{ec}\cos\omega t$ and $f_H = F_{H0} + F_{Hs}\sin\omega t + F_{Hc}\cos\omega t$, respectively. Then, express vectors

$$\begin{bmatrix} x_e & f_H \end{bmatrix}^{\mathrm{T}}, \quad \begin{bmatrix} \dot{x}_e & \dot{f}_H \end{bmatrix}^{\mathrm{T}}, \quad \begin{bmatrix} \ddot{x}_e & \ddot{f}_H \end{bmatrix}^{\mathrm{T}}, \quad \begin{bmatrix} \dddot{x}_e & \dddot{f}_H \end{bmatrix}^{\mathrm{T}} \quad \text{and} \quad \begin{bmatrix} f_e & 0 \end{bmatrix}^{\mathrm{T}}$$

as follows:

$$\begin{bmatrix} x_e \\ f_H \end{bmatrix} = \begin{bmatrix} X_{e0} \\ F_{H0} \end{bmatrix} + \sin\omega t\begin{bmatrix} X_{es} \\ F_{Hs} \end{bmatrix} + \cos\omega t\begin{bmatrix} X_{ec} \\ F_{Hc} \end{bmatrix}, \quad \begin{bmatrix} \dot{x}_e \\ \dot{f}_H \end{bmatrix} = \omega\cos\omega t\begin{bmatrix} X_{es} \\ F_{Hs} \end{bmatrix} - \omega\sin\omega t\begin{bmatrix} X_{ec} \\ F_{Hc} \end{bmatrix},$$

$$\begin{bmatrix} \ddot{x}_e \\ \ddot{f}_H \end{bmatrix} = -\omega^2\sin\omega t\begin{bmatrix} X_{es} \\ F_{Hs} \end{bmatrix} - \omega^2\cos\omega t\begin{bmatrix} X_{ec} \\ F_{Hc} \end{bmatrix}, \quad \begin{bmatrix} \dddot{x}_e \\ \dddot{f}_H \end{bmatrix} = -\omega^3\cos\omega t\begin{bmatrix} X_{es} \\ F_{Hs} \end{bmatrix} + \omega^3\sin\omega t\begin{bmatrix} X_{ec} \\ F_{Hc} \end{bmatrix},$$

$$\begin{bmatrix} f_e \\ 0 \end{bmatrix} = \begin{bmatrix} F_{e0} \\ 0 \end{bmatrix} + \sin\omega t\begin{bmatrix} F_{es} \\ 0 \end{bmatrix} + \cos\omega t\begin{bmatrix} F_{ec} \\ 0 \end{bmatrix}, \tag{15a–e}$$

where the superscript 'T' denotes the transpose.

Eq. (14) can be rewritten by substituting Eq. (15) for each vector and grouping terms into static, sine and cosine terms as

$$\begin{bmatrix} 0 & 1 \\ -k_u(X)k_r & k_u(X) \end{bmatrix}\begin{bmatrix} X_{e0} \\ F_{H0} \end{bmatrix} = \begin{bmatrix} F_{e0} \\ 0 \end{bmatrix},$$

$$\omega^3\begin{bmatrix} 0 & 0 \\ -m_{ie}c_r & 0 \end{bmatrix}\begin{bmatrix} X_{ec} \\ F_{Hc} \end{bmatrix} - \omega^2\begin{bmatrix} m_e & 0 \\ -\mu(X) & m_{ie} \end{bmatrix}\begin{bmatrix} X_{es} \\ F_{Hs} \end{bmatrix} - \omega\begin{bmatrix} 0 & 0 \\ -\gamma(X) & c_{ie} \end{bmatrix}\begin{bmatrix} X_{ec} \\ F_{Hc} \end{bmatrix} + \begin{bmatrix} 0 & 1 \\ -k_u(X)k_r & k_u(X) \end{bmatrix}\begin{bmatrix} X_{es} \\ F_{Hs} \end{bmatrix} = \begin{bmatrix} F_{es} \\ 0 \end{bmatrix},$$

$$-\omega^3\begin{bmatrix}0 & 0\\ -m_{ie}c_r & 0\end{bmatrix}\begin{bmatrix}X_{es}\\ F_{Hs}\end{bmatrix}-\omega^2\begin{bmatrix}m_e & 0\\ -\mu(X) & m_{ie}\end{bmatrix}\begin{bmatrix}X_{ec}\\ F_{Hc}\end{bmatrix}$$
$$+\omega\begin{bmatrix}0 & 0\\ -\gamma(X) & c_{ie}\end{bmatrix}\begin{bmatrix}X_{es}\\ F_{Hs}\end{bmatrix}+\begin{bmatrix}0 & 1\\ -k_u(X)k_r & k_u(X)\end{bmatrix}\begin{bmatrix}X_{ec}\\ F_{Hc}\end{bmatrix}=\begin{bmatrix}F_{ec}\\ 0\end{bmatrix}. \quad (16a-c)$$

Arrange terms to rewrite Eq. (16) as

$$\omega^3\begin{bmatrix}\mathbf{0} & \mathbf{0}\\ -m_{ie}c_r\mathbf{I} & \mathbf{0}\end{bmatrix}\begin{bmatrix}\mathbf{D}_3 & \mathbf{0}\\ \mathbf{0} & \mathbf{D}_3\end{bmatrix}\boldsymbol{\xi}+\omega^2\begin{bmatrix}m_e\mathbf{I} & \mathbf{0}\\ -\mu(X)\mathbf{I} & m_{ie}\mathbf{I}\end{bmatrix}\begin{bmatrix}\mathbf{D}_2 & \mathbf{0}\\ \mathbf{0} & \mathbf{D}_2\end{bmatrix}\boldsymbol{\xi}$$
$$+\omega\begin{bmatrix}\mathbf{0} & \mathbf{0}\\ -\gamma(X)\mathbf{I} & c_{ie}\mathbf{I}\end{bmatrix}\begin{bmatrix}\mathbf{D}_1 & \mathbf{0}\\ \mathbf{0} & \mathbf{D}_1\end{bmatrix}\boldsymbol{\xi}+\begin{bmatrix}\mathbf{0} & \mathbf{I}\\ -k_u(X)k_r\mathbf{I} & k_u(X)\mathbf{I}\end{bmatrix}\boldsymbol{\xi}=\boldsymbol{\varphi}, \quad (17)$$

where $\mathbf{I}$ and $\mathbf{0}$ are the identity matrix and the zero matrix of dimension 3, respectively, and the matrices $\mathbf{D}_1$, $\mathbf{D}_2$ and $\mathbf{D}_3$, and the vectors $\boldsymbol{\xi}$ and $\boldsymbol{\varphi}$ are defined as

$$\mathbf{D}_1=\begin{bmatrix}0 & 0 & 0\\ 0 & 0 & -1\\ 0 & 1 & 0\end{bmatrix},\quad \mathbf{D}_2=\begin{bmatrix}0 & 0 & 0\\ 0 & -1 & 0\\ 0 & 0 & -1\end{bmatrix},\quad \mathbf{D}_3=\begin{bmatrix}0 & 0 & 0\\ 0 & 0 & 1\\ 0 & -1 & 0\end{bmatrix},$$
$$\boldsymbol{\xi}=\begin{bmatrix}X_{e0} & X_{es} & X_{ec} & F_{H0} & F_{Hs} & F_{Hc}\end{bmatrix}^{\mathrm{T}},\quad \boldsymbol{\varphi}=\begin{bmatrix}F_{e0} & F_{es} & F_{ec} & 0 & 0 & 0\end{bmatrix}^{\mathrm{T}}.$$

Here, $X=X_e=\sqrt{X_{es}^2+X_{ec}^2}$. The residual formula is derived from Eq. (17) as follows:

$$\boldsymbol{\rho}(\boldsymbol{\xi},\omega)=\omega^3\begin{bmatrix}\mathbf{0} & \mathbf{0}\\ -m_{ie}c_r\mathbf{I} & \mathbf{0}\end{bmatrix}\begin{bmatrix}\mathbf{D}_3 & \mathbf{0}\\ \mathbf{0} & \mathbf{D}_3\end{bmatrix}\boldsymbol{\xi}+\omega^2\begin{bmatrix}m_e\mathbf{I} & \mathbf{0}\\ -\mu(X)\mathbf{I} & m_{ie}\mathbf{I}\end{bmatrix}\begin{bmatrix}\mathbf{D}_2 & \mathbf{0}\\ \mathbf{0} & \mathbf{D}_2\end{bmatrix}\boldsymbol{\xi}$$
$$+\omega\begin{bmatrix}\mathbf{0} & \mathbf{0}\\ -\gamma(X)\mathbf{I} & c_{ie}\mathbf{I}\end{bmatrix}\begin{bmatrix}\mathbf{D}_1 & \mathbf{0}\\ \mathbf{0} & \mathbf{D}_1\end{bmatrix}\boldsymbol{\xi}+\begin{bmatrix}\mathbf{0} & \mathbf{I}\\ -k_u(X)k_r\mathbf{I} & k_u(X)\mathbf{I}\end{bmatrix}\boldsymbol{\xi}-\boldsymbol{\varphi}. \quad (18)$$

3.3. Equation of motion for system B

Next, consider the simplified engine–mount–chassis system (B) as shown in Fig. 1(b). The governing equations consist of the following expressions and Eq. (11):

$$m_c\ddot{x}_c+c_c\dot{x}_c+k_cx_c-f_H=f_c, \quad (19)$$

$$\frac{F_H(s)}{X_e(s)-X_c(s)}=K(s,X)=k_r+c_rs+k_u(X)\frac{m_{ie}s^2+c_{ie}s}{m_{ie}s^2+c_{ie}s+k_u(X)}. \quad (20)$$

In a similar manner, the following residual formula can be derived as

$$\boldsymbol{\rho}(\boldsymbol{\xi},\omega)=\omega^3\begin{bmatrix}\mathbf{0} & \mathbf{0} & \mathbf{0}\\ \mathbf{0} & \mathbf{0} & \mathbf{0}\\ m_{ie}c_r\mathbf{I} & -m_{ie}c_r\mathbf{I} & \mathbf{0}\end{bmatrix}\begin{bmatrix}\mathbf{D}_3 & \mathbf{0} & \mathbf{0}\\ \mathbf{0} & \mathbf{D}_3 & \mathbf{0}\\ \mathbf{0} & \mathbf{0} & \mathbf{D}_3\end{bmatrix}\boldsymbol{\xi}$$
$$+\omega^2\begin{bmatrix}m_c\mathbf{I} & \mathbf{0} & \mathbf{0}\\ \mathbf{0} & m_e\mathbf{I} & \mathbf{0}\\ \mu(X)\mathbf{I} & -\mu(X)\mathbf{I} & m_{ie}\mathbf{I}\end{bmatrix}\begin{bmatrix}\mathbf{D}_2 & \mathbf{0} & \mathbf{0}\\ \mathbf{0} & \mathbf{D}_2 & \mathbf{0}\\ \mathbf{0} & \mathbf{0} & \mathbf{D}_2\end{bmatrix}\boldsymbol{\xi}$$

$$+\omega\begin{bmatrix} c_c\mathbf{I} & \mathbf{0} & \mathbf{0} \\ \mathbf{0} & \mathbf{0} & \mathbf{0} \\ \gamma(X)\mathbf{I} & -\gamma(X)\mathbf{I} & c_{ie}\mathbf{I} \end{bmatrix}\begin{bmatrix} \mathbf{D}_1 & \mathbf{0} & \mathbf{0} \\ \mathbf{0} & \mathbf{D}_1 & \mathbf{0} \\ \mathbf{0} & \mathbf{0} & \mathbf{D}_1 \end{bmatrix}\boldsymbol{\xi}$$
$$+\begin{bmatrix} k_c\mathbf{I} & \mathbf{0} & -\mathbf{I} \\ \mathbf{0} & \mathbf{0} & \mathbf{I} \\ k_u(X)k_r\mathbf{I} & -k_u(X)k_r\mathbf{I} & k_u(X)\mathbf{I} \end{bmatrix}\boldsymbol{\xi}-\boldsymbol{\varphi}. \tag{21}$$

Here, the vectors $\boldsymbol{\xi}$ and $\boldsymbol{\varphi}$, and the relative displacement X are defined as

$$\boldsymbol{\xi}=\begin{bmatrix} X_{c0} & X_{cs} & X_{cc} & X_{e0} & X_{es} & X_{ec} & F_{H0} & F_{Hs} & F_{Hc} \end{bmatrix}^{\mathrm{T}},$$

$$\boldsymbol{\varphi}=\begin{bmatrix} F_{c0} & F_{cs} & F_{cc} & F_{e0} & F_{es} & F_{ec} & 0 & 0 & 0 \end{bmatrix}^{\mathrm{T}},$$

$$X=\sqrt{(X_{es}-X_{cs})^2+(X_{ec}-X_{cc})^2}.$$

3.4. Nonlinear solution technique

A Newton–Raphson based continuation strategy can be effectively employed to minimize the residuals of Eqs. (18) and (21). Since this technique is well known [19–22], a brief review of the procedures we implemented is given in this section. First, solve the homotopy problem, where the "first" solution on a branch is calculated. For a prescribed value of $\omega=\omega_1$, the problem of $\widehat{\boldsymbol{\rho}}(\boldsymbol{\xi})=\boldsymbol{\rho}(\boldsymbol{\xi},\omega_1)=\mathbf{0}$ is iteratively solved using a Newton–Raphson method as follows:

$$\widehat{\boldsymbol{\rho}}\approx\widehat{\boldsymbol{\rho}}(\boldsymbol{\xi}^{(i)})+\left.\frac{\partial\widehat{\boldsymbol{\rho}}}{\partial\boldsymbol{\xi}}\right|_{\boldsymbol{\xi}^{(i)}}(\boldsymbol{\xi}-\boldsymbol{\xi}^{(i)})=\widehat{\boldsymbol{\rho}}(\boldsymbol{\xi}^{(i)})+\left.\frac{\partial\widehat{\boldsymbol{\rho}}}{\partial\boldsymbol{\xi}}\right|_{\boldsymbol{\xi}^{(i)}}\Delta\boldsymbol{\xi}^{(i)}=\widehat{\boldsymbol{\rho}}(\boldsymbol{\xi}^{(i)})+\widehat{\boldsymbol{\rho}}_{\boldsymbol{\xi}}(\boldsymbol{\xi}^{(i)})\Delta\boldsymbol{\xi}^{(i)}=\mathbf{0},$$
$$\boldsymbol{\xi}^{(i+1)}=\boldsymbol{\xi}^{(i)}+\Delta\boldsymbol{\xi}^{(i)}=\boldsymbol{\xi}^{(i)}-\widehat{\boldsymbol{\rho}}_{\boldsymbol{\xi}}^{-1}(\boldsymbol{\xi}^{(i)})\widehat{\boldsymbol{\rho}}(\boldsymbol{\xi}^{(i)}), \tag{22a, b}$$

where $\boldsymbol{\xi}^{(i)}$ is the ith guess.

Second, determine the tangent predictor $\begin{bmatrix} \mathrm{d}\boldsymbol{\xi}/\mathrm{d}y & \mathrm{d}\omega/\mathrm{d}y \end{bmatrix}^{\mathrm{T}}$ satisfying Eqs. (23)–(24) where y is the arc length (a new parameter) and m is the dimension of vector $\boldsymbol{\xi}$ as

$$\mathbf{0}=\boldsymbol{\rho}_{\boldsymbol{\xi}}\frac{\mathrm{d}\boldsymbol{\xi}}{\mathrm{d}y}+\boldsymbol{\rho}_{\omega}\frac{\mathrm{d}\omega}{\mathrm{d}y}, \tag{23}$$

$$\sum_{i=1}^{m}\left(\frac{\mathrm{d}\xi_i}{\mathrm{d}y}\right)^2+\left(\frac{\mathrm{d}\omega}{\mathrm{d}y}\right)^2=1. \tag{24}$$

The tangent predictor can be determined as the last column of the orthonormal matrix $\boldsymbol{Q}$ by using the QR decomposition on the transpose of the augmented non-square Jacobian $\mathbf{J}=[\boldsymbol{\rho}_{\boldsymbol{\xi}} \quad \boldsymbol{\rho}_{\omega}]$ [23]. Finally, iteratively solve $\boldsymbol{\rho}(\boldsymbol{\xi},\omega)=\mathbf{0}$ by obtaining the initial guess with the tangent predictor and an appropriate step length $\mathrm{d}y$. Use the Newton–Raphson method again as follows where $\omega^{(i)}$ is the ith guess and $\mathbf{J}^{+}$ is the pseudo-inverse of $\mathbf{J}$:

$$\boldsymbol{\rho}\approx\boldsymbol{\rho}(\boldsymbol{\xi}^{(i)},\omega^{(i)})+\boldsymbol{\rho}_{\boldsymbol{\xi}}(\boldsymbol{\xi}^{(i)},\omega^{(i)})(\boldsymbol{\xi}-\boldsymbol{\xi}^{(i)})+\boldsymbol{\rho}_{\omega}(\boldsymbol{\xi}^{(i)},\omega^{(i)})(\omega-\omega^{(i)})$$
$$=\boldsymbol{\rho}(\boldsymbol{\xi}^{(i)},\omega^{(i)})+\mathbf{J}(\boldsymbol{\xi}^{(i)},\omega^{(i)})\begin{bmatrix}\Delta\boldsymbol{\xi}^{(i)}\\ \Delta\omega^{(i)}\end{bmatrix}=\mathbf{0},$$

$$\begin{bmatrix} \xi^{(i+1)} \\ \omega^{(i+1)} \end{bmatrix} = \begin{bmatrix} \xi^{(i)} \\ \omega^{(i)} \end{bmatrix} + \begin{bmatrix} \Delta\xi^{(i)} \\ \Delta\omega^{(i)} \end{bmatrix} = \begin{bmatrix} \xi^{(i)} \\ \omega^{(i)} \end{bmatrix} - \mathbf{J}^{+}(\xi^{(i)}, \omega^{(i)})\boldsymbol{\rho}(\xi^{(i)}, \omega^{(i)}). \quad (25a,b)$$

3.5. Nonlinear frequency responses of system A

For the sake of illustration, consider the following numerical values for the system A: $m_e = 120\,\text{kg}$; $F_{e0} = 0\,\text{N}$ and $F_{es} = 0\,\text{N}$, that is, $f_e = F_{ec}\cos\omega t = F_e\cos\omega t$. Fig. 5 shows the linear frequency response functions (with constant k_u) and the nonlinear frequency responses (with $k_u(X)$ of third-order polynomial), which are normalized with respect to the excitation amplitude. Implication of a constant k_u means that the

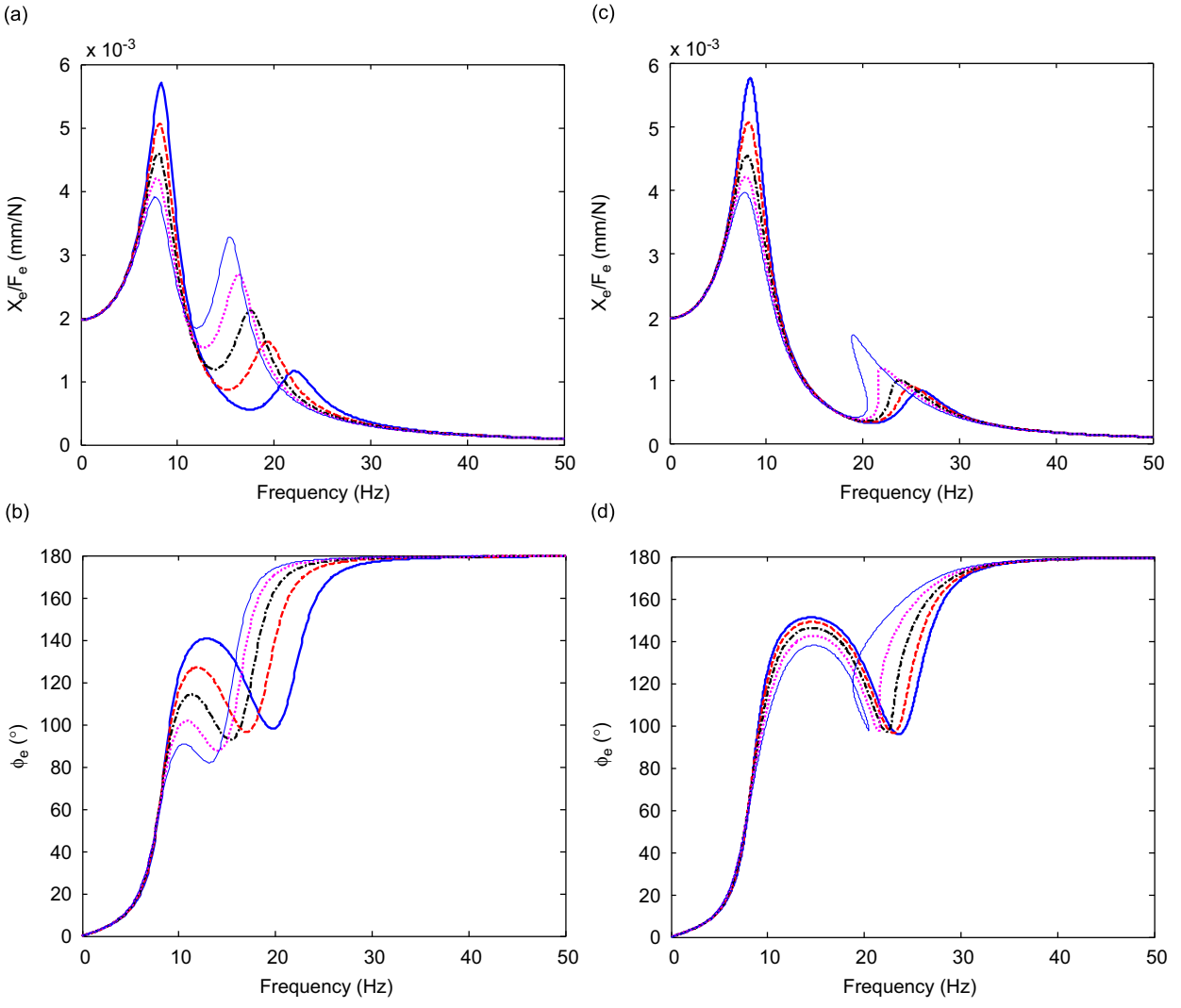

Fig. 5. Linear frequency response functions and normalized nonlinear frequency responses for system A with inertia track mount. (a) Magnitude spectra of linear frequency response functions. (b) Phase spectra of linear frequency response functions. Key: ——, k_u at $X = 0.5\,\text{mm}$ p–p; – – –, k_u at $X = 1.0\,\text{mm}$ p–p; — · —, k_u at $X = 1.5\,\text{mm}$ p–p; ·····, k_u at $X = 2.0\,\text{mm}$ p–p; ——, k_u at $X = 2.5\,\text{mm}$ p–p. (c) Magnitudes of normalized nonlinear frequency responses with $k_u(X)$ of third-order polynomial. (d) Phases of normalized nonlinear frequency responses with $k_u(X)$ of third-order polynomial. Key: ——, $X_{\max} = 0.5\,\text{mm}$ p–p; – – –, $X_{\max} = 1.0\,\text{mm}$ p–p; — · —, $X_{\max} = 1.5\,\text{mm}$ p–p; ·····, $X_{\max} = 2.0\,\text{mm}$ p–p; ——, $X_{\max} = 2.5\,\text{mm}$ p–p.

spectrally varying stiffness $K(\omega)$ is employed in the system equation, instead of $K(\omega, X)$. Comparison shows that the frequency responses at the second resonance are quite different, though they are nearly identical at the first resonance. Accordingly, the frequency response up to the first resonance regime can be accurately predicted by the linear model with $K(\omega)$ when the magnitude of response is known *a priori* to some extent. However, the difference between two formulations around the second resonance regime illustrates why the nonlinear scheme with $K(\omega, X)$ should be introduced. Observe the softening effect in Fig. 5(c), as expected from the dependence of k_u on X as shown in Fig. 4.

Fig. 6 compares the normalized nonlinear and linear frequency responses by using two *ad hoc* methods in order to illustrate their limitations. Constant stiffness k and viscous damping coefficient c values corresponding to the Kelvin–Voigt model (a spring in parallel with a viscous damper) [24] were selected from $K(\omega, X)$ data at $X \approx X_{e\max}$ at a frequency where a peak of the normalized nonlinear frequency response was evident. The spectrally varying stiffness $K(\omega)$ was selected by taking k_u as a constant at $X \approx X_{e\max}$. The frequency responses with the Kelvin–Voigt model are similar to those with $K(\omega, X)$ at the particular frequency and the amplitude where k and c were selected. However, one could not find another peak with this *ad hoc* method. Although the second peak is observed by employing the linear model with $K(\omega)$, its frequency and magnitude are not accurate. This example clearly shows that one should interpret results yielded by the two *ad hoc* methods with extreme caution.

3.6. Nonlinear frequency responses of system B

Consider the following numerical values for system B (in addition to those selected for system A): $m_c = 270\,\text{kg}$, $k_c = 20 \times 10^3\,\text{N m}^{-1}$ and $c_c = 1400\,\text{N s m}^{-1}$; $F_{c0} = 0\,\text{N}$, $F_{cs} = 0\,\text{N}$, $F_{e0} = 0\,\text{N}$ and $F_{es} = 0\,\text{N}$, that is, $f_c = F_{cc}\cos\omega t = F_c\cos\omega t$ (& $f_e = 0$) or $f_e = F_{ec}\cos\omega t = F_e\cos\omega t$ (& $f_c = 0$). Fig. 7 shows the linear frequency response functions with $K(\omega)$ where k_u is constant and Fig. 8 shows the normalized nonlinear frequency responses with $K(\omega, X)$ where $k_u(X)$ is a third-order polynomial. The nonlinear effects can be lucidly observed at the third resonance, while the linear and nonlinear frequency responses are nearly identical at the first mode. Comparison of Fig. 8(b) and (c) confirms that the reciprocity is not applicable for the nonlinear frequency responses, more specifically with the dash–dotted lines. This is expected from Fig. 9 and the maxima of the relative displacement X are observed at different modes according to the amplitude and physical location of the external force. The polynomial order of $k_u(X)$ also affects the mapping of maxima in

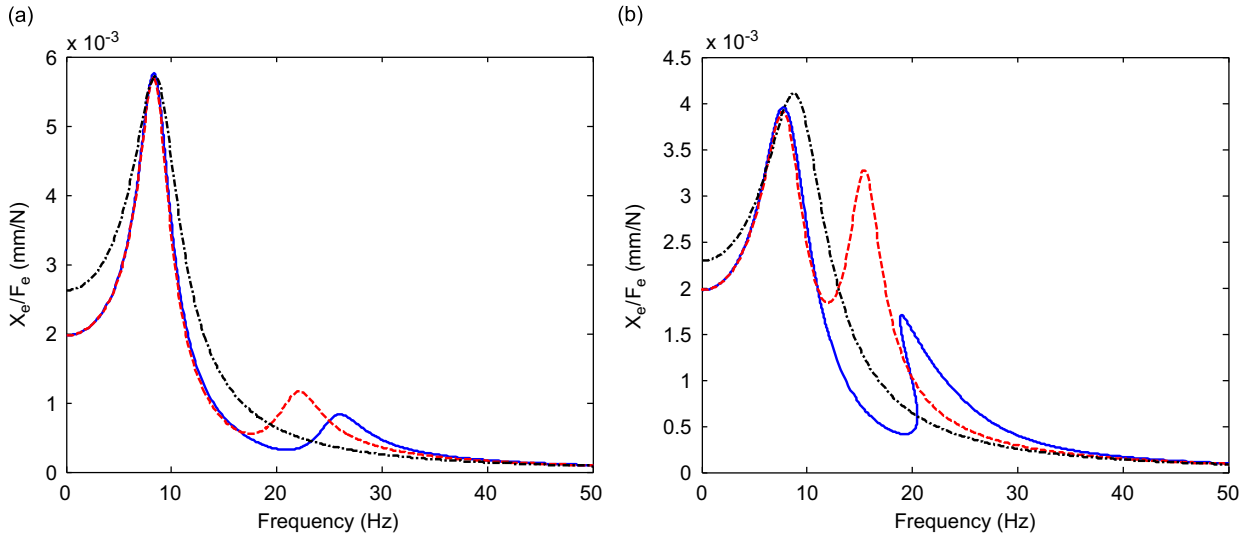

Fig. 6. Normalized nonlinear and linear frequency responses for system A with inertia track mount: (a) $X_{e\max} = 0.5\,\text{mm}$ p–p and (b) $X_{e\max} = 2.5\,\text{mm}$ p–p. Key: ——, $K(\omega, X)$; – – –, $K(\omega)$; — · —, Kelvin–Voigt model.

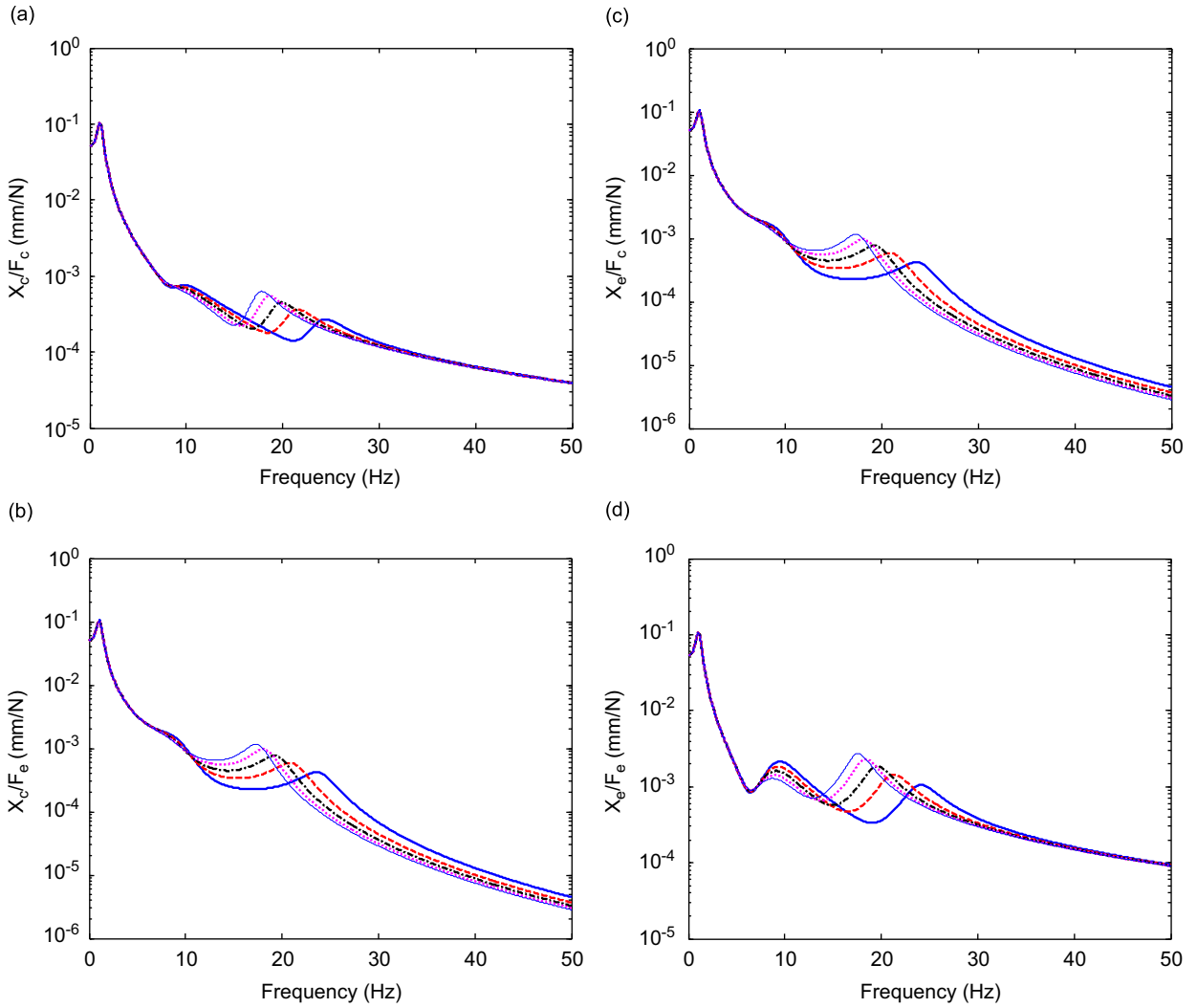

Fig. 7. Linear frequency response functions for system B with inertia track mount: (a) X_c/F_c, (b) X_c/F_e, (c) X_e/F_c and (d) X_e/F_e. Key: ——, k_u at $X = 0.5$ mm p–p; – – – –, k_u at $X = 1.0$ mm p–p; — · —, k_u at $X = 1.5$ mm p–p; ·····, k_u at $X = 2.0$ mm p–p; ——, k_u at $X = 2.5$ mm p–p.

terms of their magnitudes and frequencies. For instance, the peak value ($X_{\max} = 1.5$ mm p–p; $f_c = 0$ and $f_e = F_e \cos \omega t$) is located at the first mode for the second-order polynomial of X (the dash–dotted line in Fig. 9(c)), but it shifts to the third mode with the third-order polynomial as shown in Fig. 9(b). For system A, the maxima of the absolute displacement X are found at the first mode irrespective of input force amplitude and stiffness polynomial order as shown in Fig. 10.

3.7. Numerical issues

Some numerical issues such as the convergence, effect of frequency sweep direction and effect of a change in the force and motion units are briefly discussed. To begin with, we found that the convergence results were polynomial-order dependent. We repeated nonlinear frequency response calculations with first- to fourth-order polynomials. Non-convergent solutions were obtained with large force amplitudes, though solutions always converged, regardless of polynomial order, as long as the force amplitude is small. To overcome the numerical problems, we investigated the effect of frequency sweep direction and a change in the units of

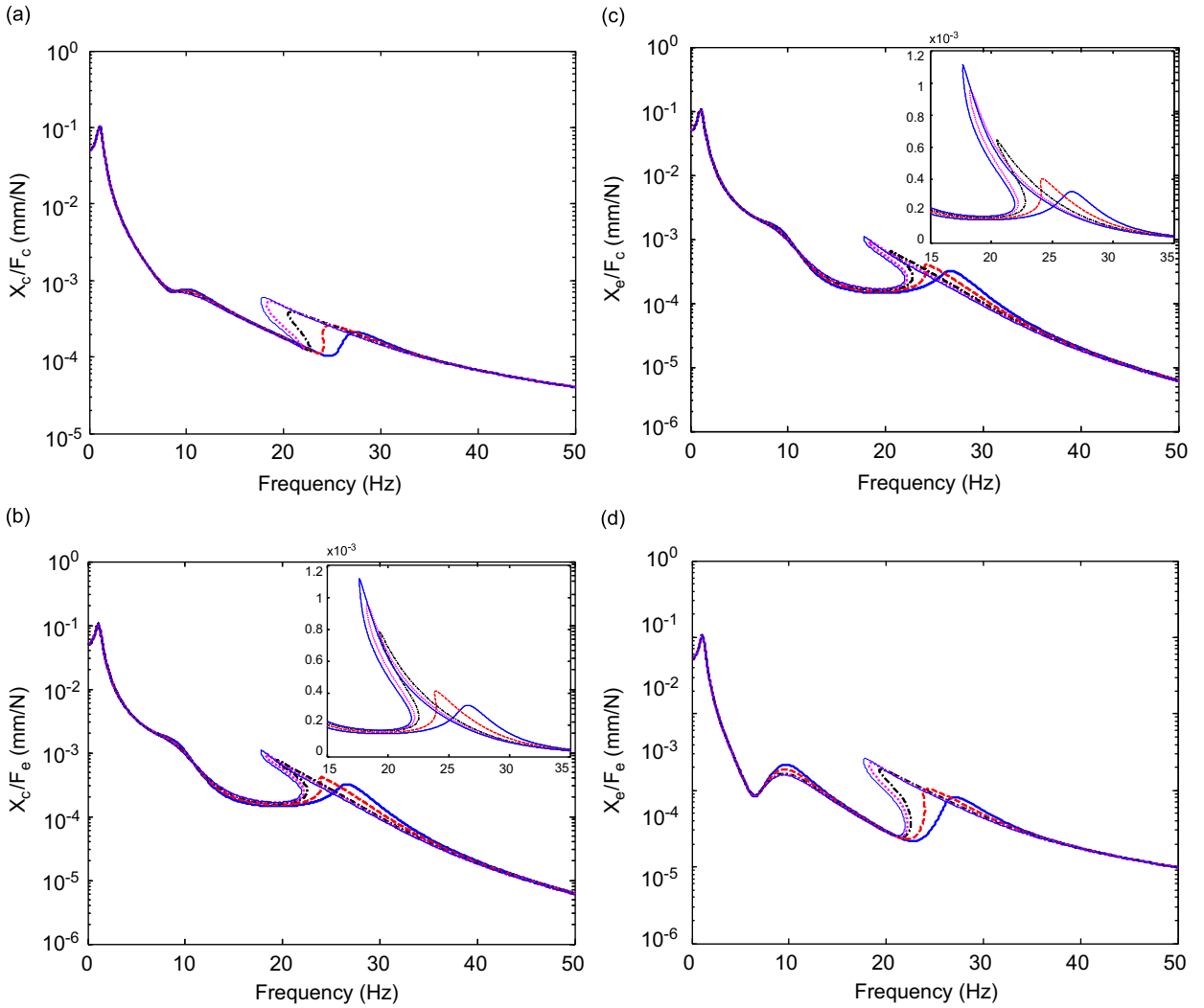

Fig. 8. Normalized nonlinear frequency responses for system B with inertia track mount: (a) X_c/F_c, (b) X_c/F_e, (c) X_e/F_c and (d) X_e/F_e. Key: ——, $X_{\max} = 0.5$ mm p–p; – – – –, $X_{\max} = 1.0$ mm p–p; —·—, $X_{\max} = 1.5$ mm p–p; ·····, $X_{\max} = 2.0$ mm p–p; ——, $X_{\max} = 2.5$ mm p–p.

calculations (for instance, from N to 10^{-3} N and from m to 10^{-3} m) on the convergence. We obtained nearly identical results when changing the frequency sweep direction or force and motion units. Finally, the computational time for the nonlinear analysis (for system B) is about 20 s on a laptop (with the 1.66 GHz dual core processor).

4. Semi-analytical solutions for systems with free decoupler mount

4.1. Quasi-linear model of free decoupler mount

Consider Eqs. (2)–(7) of the fluid model again for free decoupler mount. The transfer function can be derived as follows using Eqs. (2), (3), (5)–(7) with $I_d = 0$:

$$K(s) = k_r + c_r s + k_u c_{de} \frac{m_{ie}s^2 + c_{ie}s}{m_{ie}c_{de}s^2 + (c_{ie}c_{de} + k_u m_{ie})s + k_u(c_{ie} + c_{de})}. \tag{26}$$

where c_{de} is defined as $c_{de} = A_p^2 R_d$.

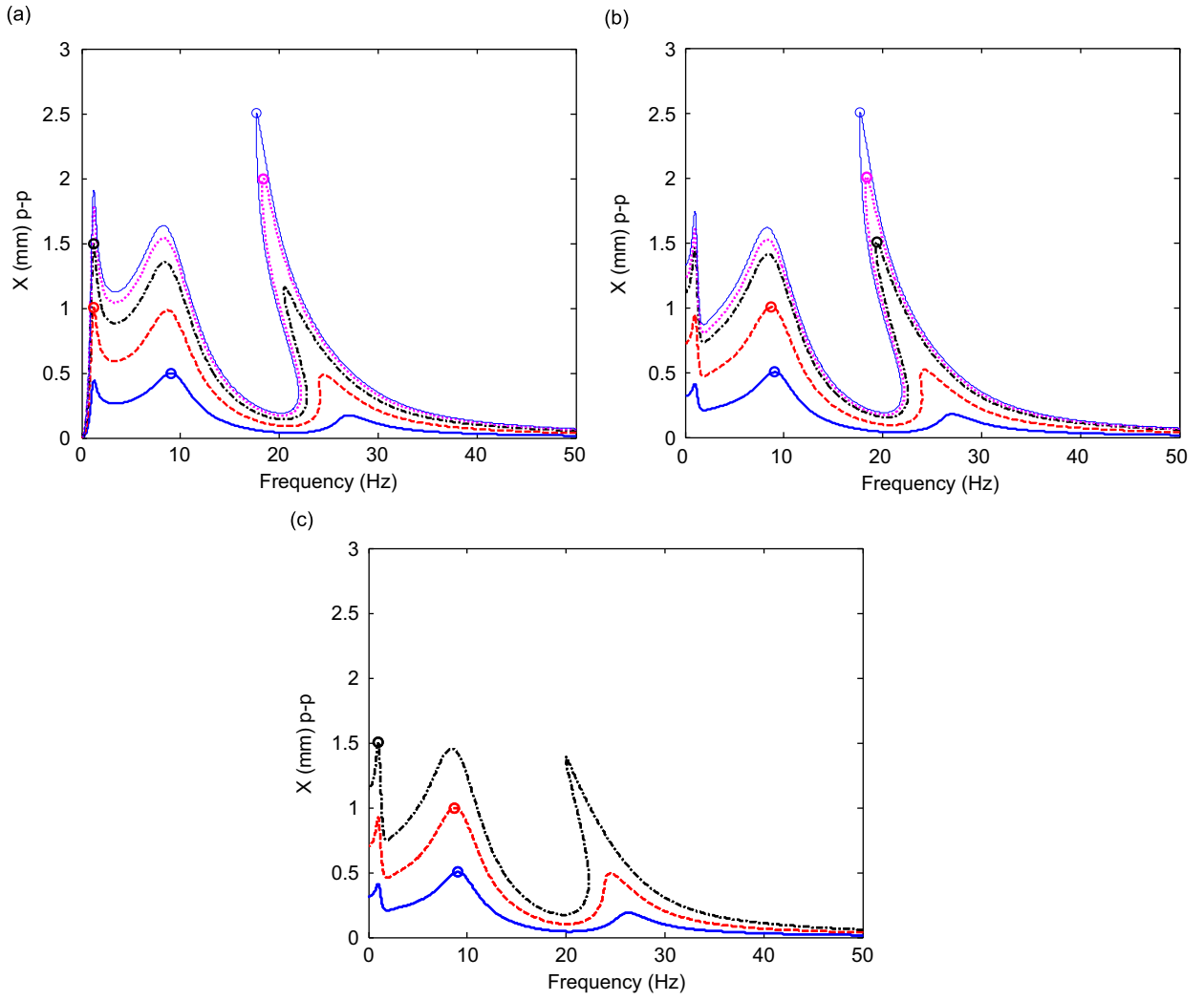

Fig. 9. Nonlinear frequency responses (in terms of relative displacements X) for system B with inertia track mount: (a) $f_c = F_c \cos \omega t$ and $f_e = 0$ ($k_u(X)$ of third-order polynomial), (b) $f_c = 0$ and $f_e = F_e \cos \omega t$ ($k_u(X)$ of third-order polynomial) and (c) $f_c = 0$ and $f_e = F_e \cos \omega t$ ($k_u(X)$ of second-order polynomial). Key: ——, $X_{\max} = 0.5$ mm p–p, ○, at $X_{\max}$; – – –, $X_{\max} = 1.0$ mm p–p, ○, at $X_{\max}$; — · —, $X_{\max} = 1.5$ mm p–p, ○, at $X_{\max}$; ·····, $X_{\max} = 2.0$ mm p–p, ○, at $X_{\max}$; ——, $X_{\max} = 2.5$ mm p–p, ○, at $X_{\max}$.

Since a particular resonance due to the decoupler is above 50 Hz, I_d is not considered. With the curve-fit function of Eq. (26), a quasi-linear model could be estimated from the stiffness measurements as shown in Fig. 11(a). Fig. 11(b) shows the transfer stiffness predicted by the following quasi-linear model with estimated parameters of Table 3:

$$K(s, X) = k_r(X) + c_r(X)s + \frac{k_u(X)c_{de}(X)\{m_{ie}(X)s^2 + c_{ie}(X)s\}}{m_{ie}(X)c_{de}(X)s^2 + \{c_{ie}(X)c_{de}(X) + k_u(X)m_{ie}(X)\}s + k_u(X)\{c_{ie}(X) + c_{de}(X)\}}, \quad (27)$$

where c_{de} is the equivalent damping coefficient due to decoupler.

The stiffness spectrum predicted by the quasi-linear model is in a good agreement with its corresponding measurement. Note that $k_u(X)$ does not dominate, unlike for inertia track mount. Therefore, c_{de}

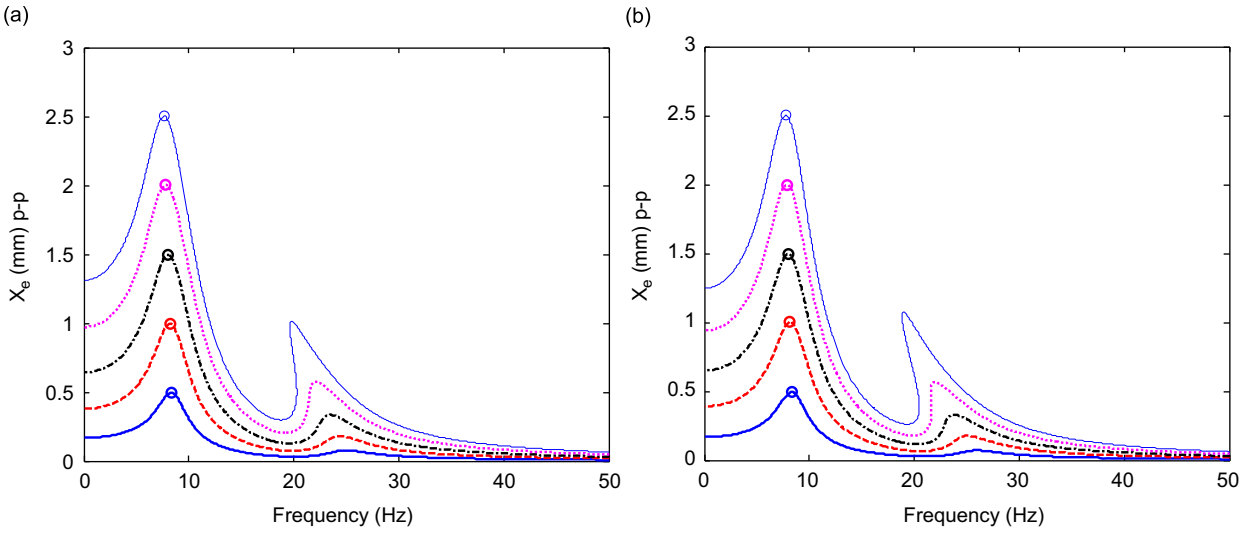

Fig. 10. Nonlinear frequency responses (in terms of absolute displacements X_e) for system A with inertia track mount: (a) $k_u(X)$ of second-order polynomial and (b) $k_u(X)$ of third-order polynomial. Key: ——, $X_{emax} = 0.5$ mm p–p, ◯, at X_{emax}; – – –, $X_{emax} = 1.0$ mm p–p, ◯, at X_{emax}; — · —, $X_{emax} = 1.5$ mm p–p, ◯, at X_{emax}; ·····, $X_{emax} = 2.0$ mm p–p, ◯, at X_{emax}; ——, $X_{emax} = 2.5$ mm p–p, ◯, at X_{emax}.

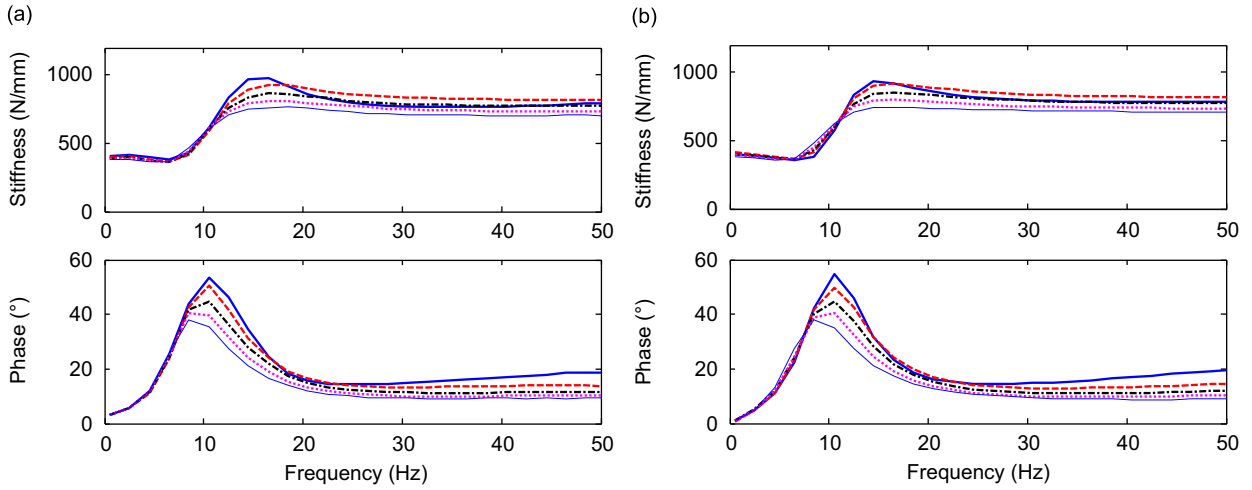

Fig. 11. Dynamic stiffness spectra of the free decoupler mount: (a) measurements and (b) predicted by the quasi-linear model given in Eq. (27). Key: ——, $X = 1.0$ mm p–p; – – –, $X = 1.5$ mm p–p; — · —, $X = 2.0$ mm p–p; ·····, $X = 2.5$ mm p–p; ——, $X = 3.0$ mm p–p.

could be regarded as a significant parameter, since an introduction of c_{de} negates the dominance of $k_u(X)$. Table 3 also shows that the ratio of c_{de}/c_{ie} is much higher than unity. Finally, the dependence of all parameters on X is estimated by curve-fitting data by using a polynomial of order n. Some parameters, however, assume negative values when $X < 1.0$ mm (p–p) with third- or fourth-order polynomial fit. Table 4 shows the associated correlation coefficients (r). Since the r value for $k_u(X)$ with first-order polynomial is too small, we will proceed with the second-order polynomials for all parameters.

Table 3
Amplitude-dependent parameters of the free decoupler mount

	X (mm) p–p				
	1.0	1.5	2.0	2.5	3.0
k_r (N mm^{-1})	403	413	400	395	383
c_r (N s m^{-1})	757	520	387	310	224
k_u (N mm^{-1})	319	365	344	319	313
m_{ie} (kg)	57.6	71.4	72.7	76.0	93.9
c_{ie} (N s m^{-1})	1370	1582	1895	1910	1913
c_{de} (N s m^{-1})	14.5×10^3	11.0×10^3	10.8×10^3	9866	8257
c_{de}/c_{ie}	10.6	7.0	5.7	5.2	4.3

Table 4
Correlation coefficients r for the parameters of free decoupler mount

Polynomial order	k_r	c_r	k_u	m_{ie}	c_{ie}	c_{de}
$n=1$	0.8330	0.9694	0.4173	0.9383	0.9042	0.9391
$n=2$	0.9407	0.9963	0.7780	0.9442	0.9835	0.9558

4.2. Equations of motion for systems A and B

For system A, the governing equations consist of Eq. (11) and

$$\frac{F_H(s)}{X_e(s)} = K(s,X) = \frac{\lambda_{21}(X)s^3 + \mu_{21}(X)s^2 + \gamma_{21}(X)s + \kappa_{21}(X)}{\mu_{22}(X)s^2 + \gamma_{22}(X)s + \kappa_{22}(X)}, \tag{28}$$

where $\lambda_{21}(X)$, $\mu_{21}(X)$, $\mu_{22}(X)$, $\gamma_{21}(X)$, $\gamma_{22}(X)$, $\kappa_{21}(X)$, and $\kappa_{22}(X)$ are defined as follows:

$$\begin{aligned}
\lambda_{21}(X) &= m_{ie}(X)c_{de}(X)c_r(X),\\
\mu_{21}(X) &= c_r(X)c_{ie}(X)c_{de}(X) + m_{ie}(X)\{k_r(X)c_{de}(X) + k_u(X)c_r(X) + k_u(X)c_{de}(X)\},\\
\mu_{22}(X) &= m_{ie}(X)c_{de}(X),\\
\gamma_{21}(X) &= k_u(X)c_r(X)\{c_{ie}(X) + c_{de}(X)\} + c_{ie}(X)c_{de}(X)\{k_r(X) + k_u(X)\}\\
&\quad + k_r(X)k_u(X)m_{ie}(X),\\
\gamma_{22}(X) &= c_{ie}(X)c_{de}(X) + k_u(X)m_{ie}(X),\\
\kappa_{21}(X) &= k_r(X)k_u(X)\{c_{ie}(X) + c_{de}(X)\}, \quad \kappa_{22}(X) = k_u(X)\{c_{ie}(X) + c_{de}(X)\}.
\end{aligned}$$

In a similar manner to Section 3.2, the residual formula is derived as

$$\begin{aligned}
\boldsymbol{\rho}(\boldsymbol{\xi},\omega) = {}& \omega^3\begin{bmatrix}\mathbf{0} & \mathbf{0}\\ -\lambda_{21}(X)\mathbf{I} & \mathbf{0}\end{bmatrix}\begin{bmatrix}\mathbf{D}_3 & \mathbf{0}\\ \mathbf{0} & \mathbf{D}_3\end{bmatrix}\boldsymbol{\xi} + \omega^2\begin{bmatrix}m_e\mathbf{I} & \mathbf{0}\\ -\mu_{21}(X)\mathbf{I} & \mu_{22}(X)\mathbf{I}\end{bmatrix}\begin{bmatrix}\mathbf{D}_2 & \mathbf{0}\\ \mathbf{0} & \mathbf{D}_2\end{bmatrix}\boldsymbol{\xi}\\
&+ \omega\begin{bmatrix}\mathbf{0} & \mathbf{0}\\ -\gamma_{21}(X)\mathbf{I} & \gamma_{22}(X)\mathbf{I}\end{bmatrix}\begin{bmatrix}\mathbf{D}_1 & \mathbf{0}\\ \mathbf{0} & \mathbf{D}_1\end{bmatrix}\boldsymbol{\xi} + \begin{bmatrix}\mathbf{0} & \mathbf{I}\\ -\kappa_{21}(X)\mathbf{I} & \kappa_{22}(X)\mathbf{I}\end{bmatrix}\boldsymbol{\xi} - \boldsymbol{\varphi}.
\end{aligned} \tag{29}$$

For system B, the governing equations consist of Eq. (11), Eq. (19) and

$$\frac{F_H(s)}{X_e(s) - X_c(s)} = K(s,X) = \frac{\lambda_{21}(X)s^3 + \mu_{21}(X)s^2 + \gamma_{21}(X)s + \kappa_{21}(X)}{\mu_{22}(X)s^2 + \gamma_{22}(X)s + \kappa_{22}(X)}. \tag{30}$$

Like Section 3.3, the following residual formula is derived as

$$\boldsymbol{\rho}(\boldsymbol{\xi},\omega)=\omega^3\begin{bmatrix}\mathbf{0}&\mathbf{0}&\mathbf{0}\\ \mathbf{0}&\mathbf{0}&\mathbf{0}\\ \lambda_{21}(X)\mathbf{I}&-\lambda_{21}(X)\mathbf{I}&\mathbf{0}\end{bmatrix}\begin{bmatrix}\mathbf{D}_3&\mathbf{0}&\mathbf{0}\\ \mathbf{0}&\mathbf{D}_3&\mathbf{0}\\ \mathbf{0}&\mathbf{0}&\mathbf{D}_3\end{bmatrix}\boldsymbol{\xi}$$
$$+\omega^2\begin{bmatrix}m_c\mathbf{I}&\mathbf{0}&\mathbf{0}\\ \mathbf{0}&m_e\mathbf{I}&\mathbf{0}\\ \mu_{21}(X)\mathbf{I}&-\mu_{21}(X)\mathbf{I}&\mu_{22}(X)\mathbf{I}\end{bmatrix}\begin{bmatrix}\mathbf{D}_2&\mathbf{0}&\mathbf{0}\\ \mathbf{0}&\mathbf{D}_2&\mathbf{0}\\ \mathbf{0}&\mathbf{0}&\mathbf{D}_2\end{bmatrix}\boldsymbol{\xi}$$
$$+\omega\begin{bmatrix}c_c\mathbf{I}&\mathbf{0}&\mathbf{0}\\ \mathbf{0}&\mathbf{0}&\mathbf{0}\\ \gamma_{21}(X)\mathbf{I}&-\gamma_{21}(X)\mathbf{I}&\gamma_{22}(X)\mathbf{I}\end{bmatrix}\begin{bmatrix}\mathbf{D}_1&\mathbf{0}&\mathbf{0}\\ \mathbf{0}&\mathbf{D}_1&\mathbf{0}\\ \mathbf{0}&\mathbf{0}&\mathbf{D}_1\end{bmatrix}\boldsymbol{\xi}$$
$$+\begin{bmatrix}k_c\mathbf{I}&\mathbf{0}&-\mathbf{I}\\ \mathbf{0}&\mathbf{0}&\mathbf{I}\\ \kappa_{21}(X)\mathbf{I}&-\kappa_{21}(X)\mathbf{I}&\kappa_{22}(X)\mathbf{I}\end{bmatrix}\boldsymbol{\xi}-\boldsymbol{\varphi}. \tag{31}$$

4.3. Nonlinear frequency responses of systems A and B

Figs. 12(a) and 13 show the linear frequency response functions of systems A and B, respectively, by taking all parameters as constants. Figs. 12(b) and 14 present the normalized nonlinear frequency responses of both systems where all mount parameters are given by the second-order polynomial of X. Observe that the nonlinear behavior with free decoupler mount differs sharply from that with inertia track mount. While the softening nonlinearity is clearly observed with inertia track mount, it is not seen in the nonlinear response with free decoupler mount. Furthermore, peaks of the relative displacement X for system B with free decoupler

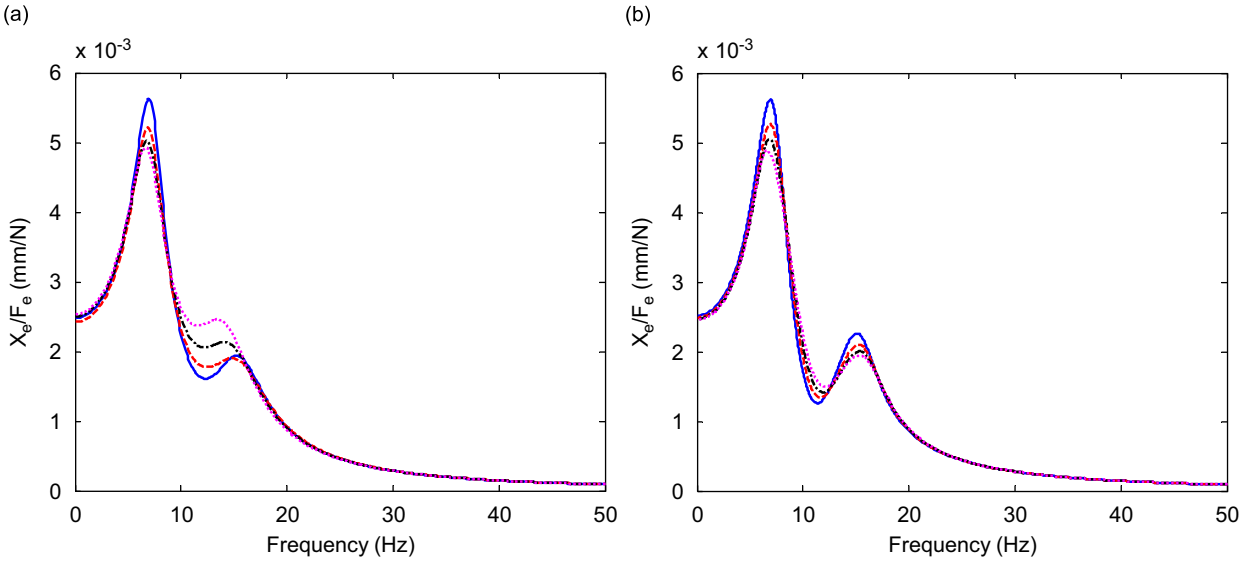

Fig. 12. Frequency responses for system A with free decoupler mount. (a) Linear frequency response functions with constant parameters. Key: ——, $X=1.0$ mm p–p; – – – –, $X=1.5$ mm p–p; — · —, $X=2.0$ mm p–p; ·····, $X=2.5$ mm p–p. (b) Normalized nonlinear frequency responses with amplitude-dependent parameters (of second-order polynomial). Key: ——, $X_{\max}=1.0$ mm p–p; – – – –, $X_{\max}=1.5$ mm p–p; — · —, $X_{\max}=2.0$ mm p–p; ·····, $X_{\max}=2.5$ mm p–p.

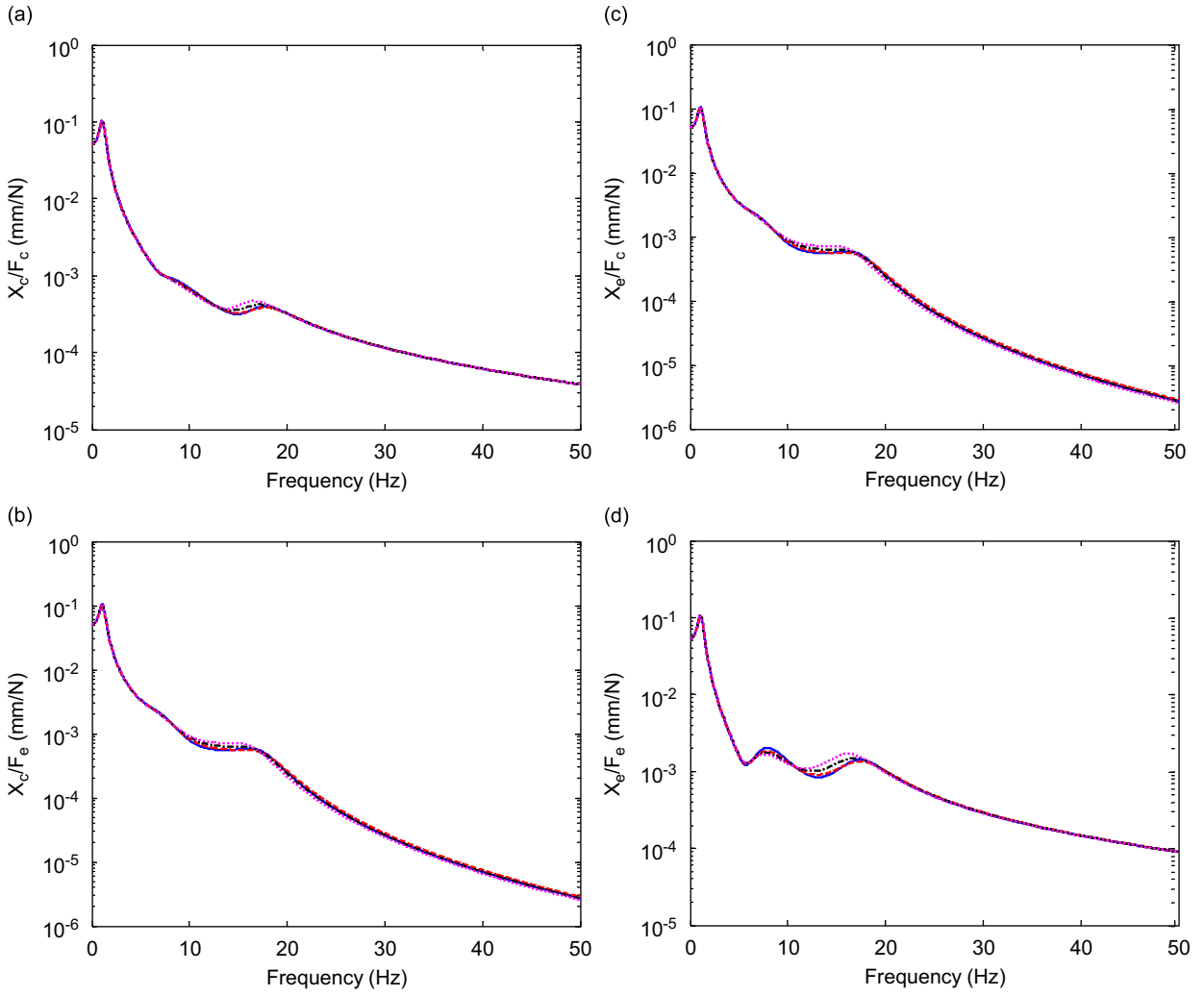

Fig. 13. Linear frequency response functions for system B with free decoupler mount: (a) X_c/F_c, (b) X_c/F_e, (c) X_e/F_c and (d) X_e/F_e. Key: ——, $X = 1.0$ mm p–p; – – –, $X = 1.5$ mm p–p; — · —, $X = 2.0$ mm p–p; ·····, $X = 2.5$ mm p–p.

mount are found at the first mode irrespective of the amplitude and physical location of the external force unlike the case of system B with inertia track mount. In fact, nonlinear frequency responses of system B with free decoupler mount resemble responses of a linear time-invariant system. Reciprocity and lack of amplitude sensitivity are seen for this case, probably due to high damping c_{de} introduced by the decoupler.

5. Conclusion

Our analysis shows that the proposed scheme should be employed, instead of the *ad hoc* methods, when the mount parameters exhibit amplitude sensitivity. In particular, the inclusion of inertia track mount leads to the softening effect in both systems (A and B). Fig. 15 shows the nonlinear frequency responses and local maxima. The associated backbone curves can be inferred from the locus of local maxima. The backbone curve for system A (at the second mode) is a straight line with a negative slope (solid line in Fig. 16). Conversely, the left half of a convex curve for system B (around the third mode) is also shown (dashed line) in Fig. 16.

To qualitatively assess the underlying physics, we examine two well-known differential equations with cubic and asymmetric nonlinearities as stated below. Both equations with positive β yield softening nonlinearity

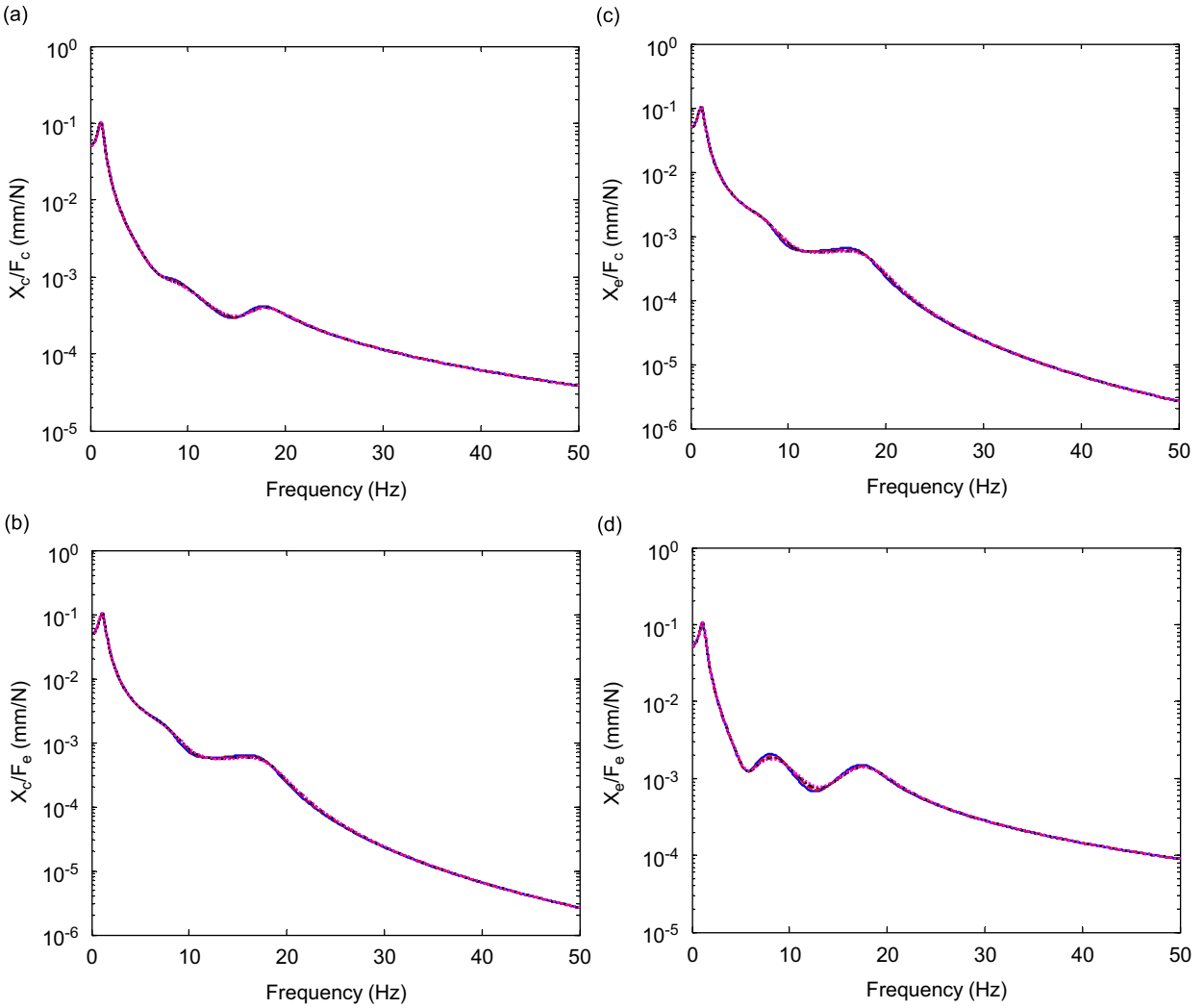

Fig. 14. Normalized nonlinear frequency responses for system B with free decoupler mount. (a) X_c/F_c. (b) X_c/F_e. (c) X_e/F_c. (d) X_e/F_e. Key: ——, $X_{\max} = 1.0$ mm p–p; – – –, $X_{\max} = 1.5$ mm p–p; — · —, $X_{\max} = 2.0$ mm p–p; ·····, $X_{\max} = 2.5$ mm p–p.

under the harmonic excitation:

$$m\ddot{x} + c\dot{x} + kx(1 - \beta x^2) = F\cos\omega t, \tag{32}$$

$$m\ddot{x} + c\dot{x} + kx(1 - \beta|x|) = F\cos\omega t. \tag{33}$$

Further, the backbone curves of Eqs. (32) and (33) are expressed via the method of iteration [14] and the describing function analysis, respectively, as below, where X is the amplitude of x and $\omega_n = \sqrt{k/m}$:

$$X = \sqrt{\frac{4}{3\beta}\left(1 - \frac{\omega^2}{\omega_n^2}\right)}, \tag{34}$$

$$X = \frac{3\pi}{8\beta}\left(1 - \frac{\omega^2}{\omega_n^2}\right). \tag{35}$$

Both Eqs. (34) and (35) predict a well-known shape (dash–dotted line in Fig. 16). However, the resulting backbone curves are quite different from those yielded by the nonlinear responses of systems A and B with

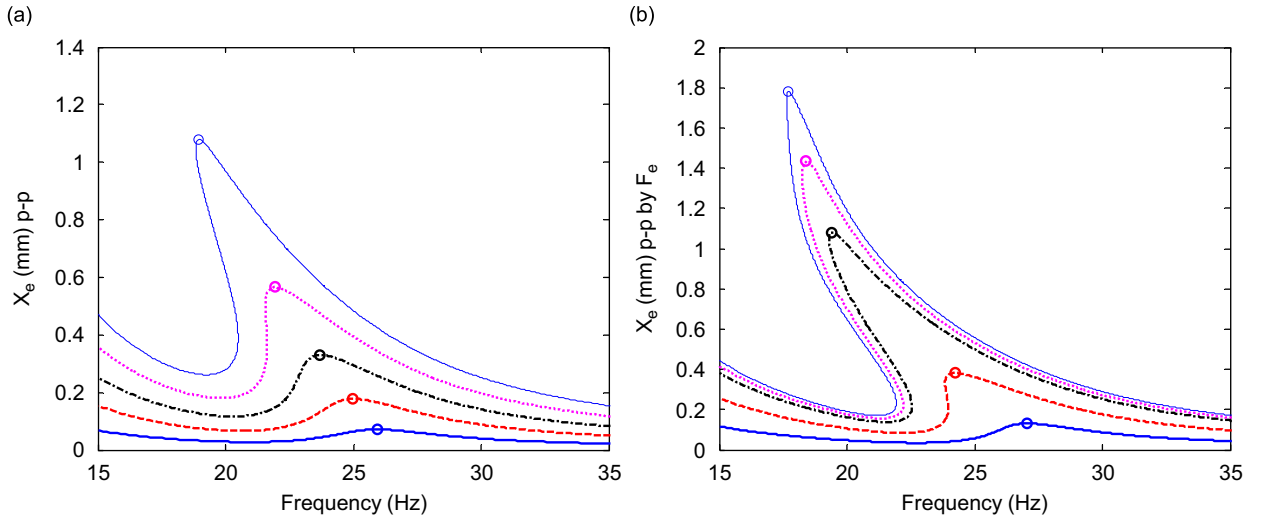

Fig. 15. Nonlinear frequency responses X_e with inertia track mount: (a) system A and (b) system B ($f_c = 0$ and $f_e = F_e \cos \omega t$). Key: ——, $X_{max} = 0.5$ mm p–p, ○, at local maximum of X_e; – – –, $X_{max} = 1.0$ mm p–p, ○, at local maximum of X_e; — · —, $X_{max} = 1.5$ mm p–p, ○, at local maximum of X_e; ·····, $X_{max} = 2.0$ mm p–p, ○, at local maximum of X_e; ——, $X_{max} = 2.5$ mm p–p, ○, at local maximum of X_e.

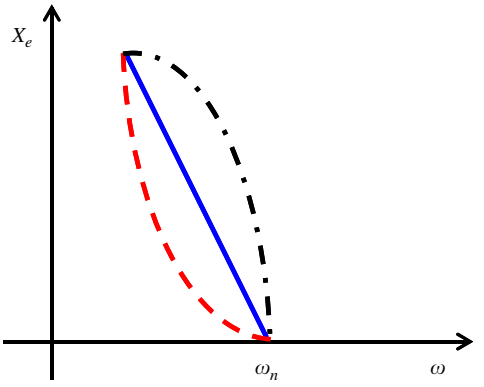

Fig. 16. Comparison of the backbone curves with classical nonlinear oscillators. Key: ——, System A with inertia track mount; – – –, System B with inertia track mount; — · —, Duffing's oscillator of Eq. (32) or asymmetric nonlinearity of Eq. (33).

inertia track mount. Based on the comparison of Fig. 16 alone, we surmise that the classical nonlinear differential equations such as Eqs. (32) and (33) cannot be readily applied to the quarter vehicle systems with amplitude-sensitive isolators (such as inertia track mounts). Moreover, one should differentiate between the amplitude-dependent $K(X)$ term and the softening spring expression $k(1 - \beta x^2)$ of Eq. (32); recall that $x(t)$ is time-varying displacement and X is the amplitude of $x(t)$. For the sake of argument, write $K(X) = k(1 - \beta X^2)$. The direct insertion of $K(X)$ into a time-domain formulation (differential equation) would pose difficulty as the formulation is valid only when the external force is purely sinusoidal. In contrast, the differential equation with $k(1 - \beta x^2)$ is valid for any force time history. Furthermore, $x(t)$ could assume positive, negative or zero values, while X is always positive and greater than zero.

System B with the free decoupler mount looks more like a linear time-invariant system, at least from the frequency response perspective. This is a surprising conclusion since the amplitude sensitivity of both mounts seems significant at the component level. In this particular design, the effect of high decoupler damping

negates the amplitude sensitivity in the frequency domain. However, we expect a different result in time domain since discontinuous nonlinearities associated with the flow switching process must be considered in time domain [15]. This work will be reported soon.

In summary, the vehicle system with a real-life nonlinear device was analyzed given limited measured mount properties in the form of $K(\omega, X)$. The one-term harmonic balance method was employed to construct nonlinear frequency responses since it is compatible with the experimental procedure used for dynamic characterization of isolators. The fundamental nature of the governing nonlinear system with $K(\omega, X)$ and associated computational issues have been clearly demonstrated. Our method could be extended to other nonlinear isolation systems.

Acknowledgments

This work was supported by the Korea Research Foundation Grant (KRF-2006-352-D00035) funded by the Government of Korea (MOEHRD).

References

[1] A.D. Nashif, D.I.G. Jones, J.P. Henderson, *Vibration Damping*, Wiley, New York, 1985.
[2] Y. Yu, N.G. Naganathan, R.V. Dukkipati, A literature review of automotive vehicle engine mounting systems, *Mechanism and Machine Theory* 36 (2001) 123–142.
[3] G. Kim, R. Singh, Nonlinear analysis of automotive hydraulic engine mount, *ASME Journal of Dynamic Systems, Measurement and Control* 115 (1993) 482–487.
[4] G. Kim, R. Singh, A study of passive and adaptive hydraulic engine mount systems with emphasis on non-linear characteristics, *Journal of Sound and Vibration* 179 (3) (1995) 427–453.
[5] J.E. Colgate, C.-T. Chang, Y.-C. Chiou, W.K. Liu, L.M. Keer, Modelling of a hydraulic engine mount focusing on response to sinusoidal and composite excitations, *Journal of Sound and Vibration* 184 (3) (1995) 503–528.
[6] A. Geisberger, A. Khajepour, F. Golnaraghi, Non-linear modeling of hydraulic mounts: theory and experiment, *Journal of Sound and Vibration* 249 (2) (2002) 371–397.
[7] T. Jeong, R. Singh, Inclusion of measured frequency- and amplitude-dependent mount properties in vehicle or machinery models, *Journal of Sound and Vibration* 245 (3) (2001) 385–415.
[8] G.N. Jazar, M.F. Golnaraghi, Nonlinear modeling, experimental verification, and theoretical analysis of a hydraulic engine mount, *Journal of Vibration and Control* 8 (2002) 87–116.
[9] M.S. Foumani, A. Khajepour, M. Durali, Application of sensitivity analysis to the development of high performance adaptive hydraulic engine mounts, *Vehicle System Dynamics* 39 (4) (2003) 257–278.
[10] M.F. Golnaraghi, G.N. Jazar, Development and analysis of a simplified nonlinear model of a hydraulic engine mount, *Journal of Vibration and Control* 7 (2001) 495–526.
[11] J. Christopherson, G.N. Jazar, Dynamic behavior comparison of passive hydraulic engine mounts. Part 1: Mathematical analysis, *Journal of Sound and Vibration* 290 (2006) 1040–1070.
[12] T.J. Royston, R. Singh, Vibratory power flow through a non-linear path into a resonant receiver, *Journal of the Acoustical Society of America* 101 (4) (1997) 2059–2069.
[13] M. Tiwari, H. Adiguna, R. Singh, Experimental characterization of a nonlinear hydraulic engine mount, *Noise Control Engineering Journal* 51 (1) (2003) 36–49.
[14] W.T. Thomson, *Theory of Vibration with Applications*, fourth ed., Prentice-Hall, Englewood Cliffs, 1993.
[15] H. Adiguna, M. Tiwari, R. Singh, H.E. Tseng, D. Hrovat, Transient response of a hydraulic engine mount, *Journal of Sound and Vibration* 268 (2003) 217–248.
[16] R. Singh, G. Kim, P.V. Ravindra, Linear analysis of automotive hydro-mechanical mount with emphasis on decoupler characteristics, *Journal of Sound and Vibration* 158 (2) (1992) 219–243.
[17] J.-H. Lee, M.-S. Bae, K.-J. Kim, Limitations of mechanical model with lumped mass in representing dynamic characteristics of hydraulic mount (SAE 2003-01-1466), *Journal of Passenger Cars—Mechanical Systems* 112 (2004) 1679–1683.
[18] S. He, R. Singh, Estimation of amplitude and frequency dependent parameters of hydraulic engine mount given limited dynamic stiffness measurements, *Noise Control Engineering Journal* 53 (6) (2005) 255–269.
[19] R. Seydel, *Practical Bifurcation and Stability Analysis: From Equilibrium to Chaos*, second ed., Springer-Verlag, New York, 1994.
[20] C. Padmanabhan, R. Singh, Analysis of periodically excited non-linear systems by a parametric continuation technique, *Journal of Sound and Vibration* 184 (1) (1995) 35–58.
[21] T.C. Kim, T.E. Rook, R. Singh, Super- and sub-harmonic response calculations for a torsional system with clearance nonlinearity using the harmonic balance method, *Journal of Sound and Vibration* 281 (2005) 965–993.

[22] T.C. Kim, T.E. Rook, R. Singh, Effect of nonlinear impact damping on the frequency response of a torsional system with clearance, *Journal of Sound and Vibration* 281 (2005) 995–1021.
[23] T.J. Royston, R. Singh, Periodic response of mechanical systems with local non-linearities using an enhanced Galerkin technique, *Journal of Sound and Vibration* 194 (2) (1996) 243–263.
[24] A.S. Wineman, K.R. Rajagopal, *Mechanical Response of Polymers: An Introduction*, Cambridge University Press, Cambridge, 2000.